Ecological Informatics 93 (2026) 103577

Contents lists available at ScienceDirect

Ecological Informatics

journal homepage: www.elsevier.com/locate/ecolinf

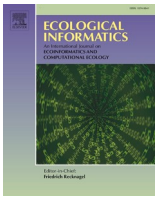

Benthic habitat influences sea scallop distributions and swimming behavior based on underwater imagery and machine learning

Liese A. Siemann [a,*], Matthew Dawkins [b], Luisa M. Garcia [a], Jonathan Crall [b], Tasha E. O'Hara [a]

[a] Coonamessett Farm Foundation, Inc., 277 Hatchville Rd., East Falmouth, MA, 02536, USA
[b] Kitware Inc., 1712 US-9 #300, Clifton Park, NY 12065, USA

ARTICLE INFO

Keywords:
HabCam
VIAME
CMECS
Scallop surveys
Image annotation
Computer vision

ABSTRACT

Understanding the drivers of Atlantic sea scallop distribution and abundance is a priority for fisheries management. While factors influencing scallop habitat selection and recruitment remain poorly understood, the increasing use of optical surveys for scallop assessment has opened new opportunities for studying juvenile and adult scallop distributions. Yet manual image annotation is time-consuming, limiting the potential of these datasets. Automating this process could improve biomass estimates and advance research on scallop ecology by enabling the analysis of larger datasets in a fraction of the time required for manual annotation. This study aimed to (1) use automated scallop detectors and benthic habitat classifiers to generate accurate scallop plus habitat datasets for large numbers of images from Habitat Mapping Camera surveys of scallop grounds and (2) use these datasets to develop models to assess how benthic habitat influences sea scallop distributions and age-specific swimming behavior. Scallop detectors and habitat classifiers were developed for the computer vision platform Video and Image Analytics for Marine Environments. Density models using automated datasets indicated that benthic habitat components (gravel, shell hash, bryozoans, sea star beds, sand dollar beds, and sand waves) influenced scallop densities, with some trends for habitat preference shifting with age. Swimming models confirmed that juvenile scallops swim more frequently than adults, particularly in areas with lower bryozoan densities. This work highlights the value of using automated tools to process large-scale optical datasets and provides new insights into habitat-specific scallop behavior across life stages.

1. Introduction

The Atlantic sea scallop, *Placopecten magellanicus*, is the focus of one of the most valuable fisheries in the eastern United States (US), with US scallop landings valued at $467 million in 2022 (NMFS, 2024). Understanding the factors that impact sea scallop distribution and abundance is therefore a key fisheries management priority. The sustainability of this fishery depends on consistent and successful recruitment from wild populations of scallops, coupled with survival of multiple age classes through adulthood across the range of this species. The factors that lead to successful recruitment, including those that impact juvenile habitat selection and survival, remain poorly understood. Larval scallops prefer to settle on substrates with three-dimensional structure such as gravel, shells, or filamentous epifauna (Cragg, 2006), but juvenile scallops can swim and settle in new areas (Brand, 2016; Carey and Stokesbury, 2011). Like adult scallops, they seem to prefer substrates from sand to gravel, and they can be found in areas with primarily juveniles or in areas with mixed assemblages of all size classes (Brand, 2016; Carey and Stokesbury, 2011). The presence of predators may strongly impact juvenile and adult scallop distributions, and as a result, the presence of heterogeneous substrate with vertical relief may affect juvenile scallop distributions by providing refuges that enhance survival through predator avoidance (Brand, 2016; Carey and Stokesbury, 2011; Wong and Barbeau, 2003).

The challenges associated with studying juvenile scallops in situ have limited the ability of researchers to better understand juvenile scallop ecology and its impacts on adult scallop distributions. Prior to 2010, dredges were the standard tools used for sea scallop surveys, and even if dredge bags were equipped with mesh liners to capture smaller scallops, these juvenile scallops often escaped detection by passing through the bags or liners or under the dredge (Carey and Stokesbury, 2011). However, the growing use of optical surveys for scallop assessment has opened new opportunities for studying juvenile and adult scallop distributions (Carey and Stokesbury, 2011). Coonamessett Farm

* Corresponding author.
E-mail address: lsiemann@cfarm.org (L.A. Siemann).

https://doi.org/10.1016/j.ecoinf.2025.103577
Received 24 May 2025; Received in revised form 15 December 2025; Accepted 19 December 2025
Available online 22 December 2025
1574-9541/© 2025 The Authors. Published by Elsevier B.V. This is an open access article under the CC BY license (http://creativecommons.org/licenses/by/4.0/).

Foundation (CFF) has a multi-year database of imagery from scallop surveys using the Habitat Mapping Camera (HabCam) V3 (**Appendix A**). This system collects four to six images per second as it is towed along predetermined tracks within scallop fishing grounds, providing a continuous track of overlapping imagery. Each image includes associated metadata with location (latitude and longitude), vehicle pose (altitude, pitch, and roll) and environmental data (depth, bottom temperature, and conductivity/salinity). Annotations from these images are used to generate abundance and distribution maps of scallops by size class, highlighting locations where juvenile and adult scallops are found year to year. Annotations are also used to estimate biomass by converting scallop lengths in pixels to shell heights in millimeters using the field of view (FOV) of each image. Each shell height (SH) measured from the HabCam images is converted to a meat weight (MW) in grams using published location-specific SHMW equations (e.g., Hennen and Hart, 2012). Biomass in a defined stock area is estimated using a combination of expanded means, kriging, and/or mixed models to generate the data needed for stock assessment projections (Chang et al., 2017; NEFSC, 2018).

Manual image annotation is the most time-consuming aspect of generating scallop distribution maps and biomass estimates from optical survey imagery, often resulting in less than 1 % to 10 % of images being annotated per survey. Increased annotation rates would improve confidence in biomass estimates and enhance the detection of sparsely settled target organisms, including pre-recruit scallops (Carey and Stokesbury, 2011). Reliably automating image annotation has the potential to substantially increase annotation rates for optical scallop surveys, leading to more accurate biomass estimates and addressing emerging questions regarding scallop patchiness and distribution over small-to-large scales within scallop grounds. Moreover, manual annotations of benthic substrates are often inconsistent, as substrate and habitat classification can vary among annotators, reducing comparability across surveys. Automating both scallop detection and habitat classification offers a practical solution to these challenges by greatly increasing annotation quantity and improving consistency in defining habitat characteristics. This approach enhances the accuracy of scallop biomass estimates and promotes a clearer understanding of relationships between scallop distribution, swimming behavior, and benthic habitat features across spatial scales. Based on these considerations, the aims of this study were to 1) use automated detectors for scallops and automated classifiers for benthic habitat to generate accurate scallop plus habitat datasets for large numbers of images using computational neural networks and 2) use datasets from these automated detectors and classifiers to develop models to investigate the impacts of benthic habitat on sea scallop distributions and swimming behavior by age class, focusing on age classes from recently settled juveniles through adults.

2. Methods

The images used to generate the data for this study were collected during the 2019 and 2021 sea scallop surveys conducted by CFF. These surveys included scallop grounds on Georges Bank and in the Mid-Atlantic Bight, covering most known sea scallop grounds along the East Coast of the US (Fig. 1). Details about the HabCam V3 vehicle, sensors, and survey operations are included in **Appendix A**.

2.1. Applying scallop detectors and benthic habitat classifiers

Scallop detectors and habitat classifiers developed in Video and Image Analytics for Marine Environments (VIAME) were used to process 1,369,890 images from the 2019 and 2021 HabCam surveys. These images were not used during development of the scallop detectors or benthic habitat classifiers. VIAME is an open-source computer vision platform for analysis of underwater imagery (Dawkins et al., 2017), and CFF has worked with the developers to incorporate scallop and habitat models into the packages available on the platform. The scallop detectors label scallops as live scallops (i.e., scallops resting on the seafloor) and swimming scallops (Fig. 2), distinguishing these from dead scallops or clappers (i.e., shells with intact hinges). Scallop sizes can be estimated using image metadata or depth maps from paired stereo images. The habitat classifiers are based on the Coastal and Marine Ecological Classification Standard (CMECS), a standard framework for describing and classifying ecological units, including geoforms, substrate, and biotic components (Allee et al., 2012). Six habitat components were included in the datasets (Table 1). These included habitat components that can impact scallop settlement (gravel, shell, and

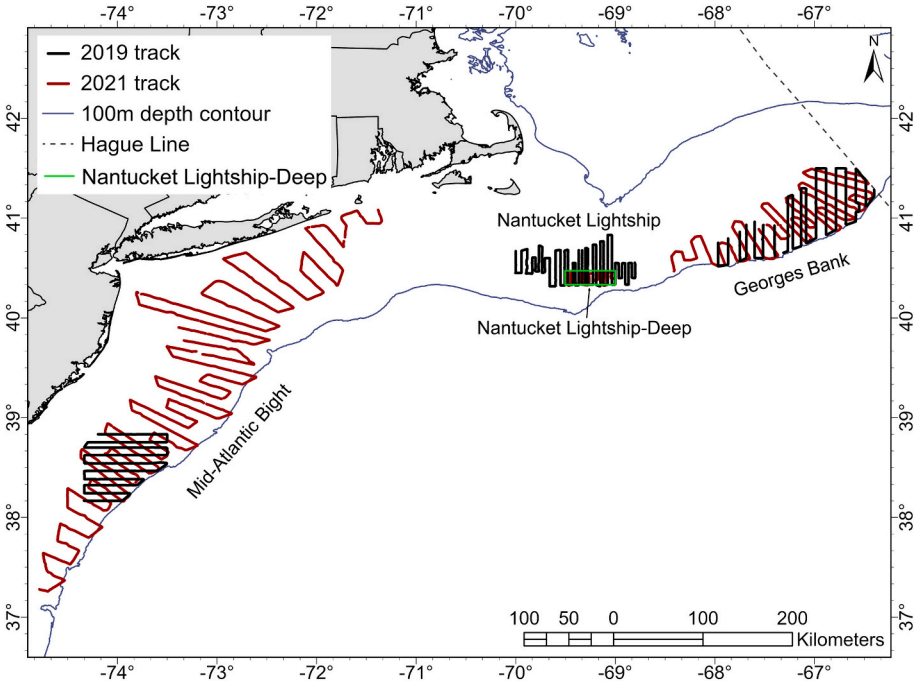

Fig. 1. Map of the 2019 and 2021 HabCam V3 survey tracks over the scallop grounds on Georges Bank and in the Mid-Atlantic Bight.

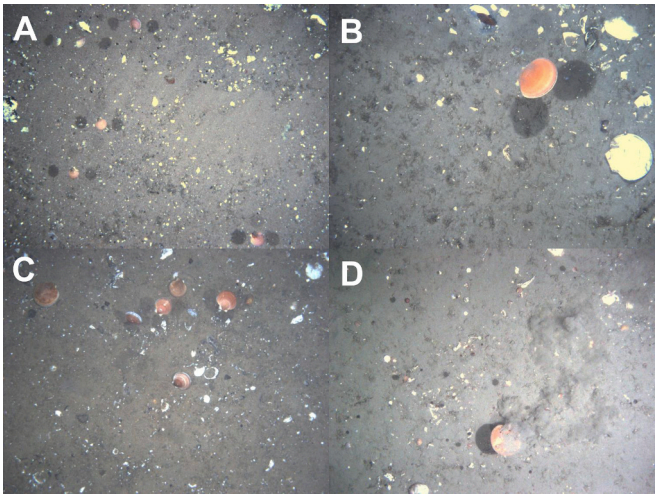

Fig. 2. Examples of swimming scallops. Swimming scallops can be differentiated from other live scallops based on (A-B) shadows from the HabCam vehicle lights, (C) orientation with the shell opening facing up toward the camera, and (D) the presence of a sediment cloud formed by scallop jet propulsion.

Table 1
Substrate, biotic, and geoform components used for habitat classifications. The null or reference class is the first category listed.

Habitat component	CMECS level: class	Categories	Image coverage percentage and/or count
Gravel	Substrate: unconsolidated mineral substrate	mud/sand	<5 % gravel
		gravelly gravel	5–30 % gravel
			>30 % gravel
Shell	Substrate: shell	no shell hash	<5 % shell hash
		shell hash sparse	5–30 % shell hash
		shell hash	30–80 % shell hash
		shell hash dense	>80 % shell hash
Bryozoans	Biotic: attached bryozoans	no bryozoans	<5 % bryozoans
		bryozoans sparse	5–30 % bryozoans
		bryozoans	30–80 % bryozoans
		bryozoans dense	>80 % bryozoans
Sea stars	Biotic: attached starfish	no sea stars	<10 sea stars
		sea star bed	≥50 % sea star coverage or ≥ 10 sea stars
Sand dollars	Biotic: sand dollar bed	no sand dollars	<10 sand dollars
		sand dollar bed	≥50 % sand dollar coverage or ≥ 10 sand dollars
Sand waves	Geoform: megaripples	no sand waves	<50 % sand waves
		sand waves	≥50 % sand waves

bryozoans; Cragg, 2006), beds of echinoderms that may influence scallop distributions (Rosellon-Druker and Stokesbury, 2019), and sand waves and ripples as indicators of strong bottom currents (Fig. 3). Images were classified for each component independently, allowing habitat to be classified based on multiple characteristics. Details about the development of the scallop detectors and habitat classifiers are included in **Appendix B**.

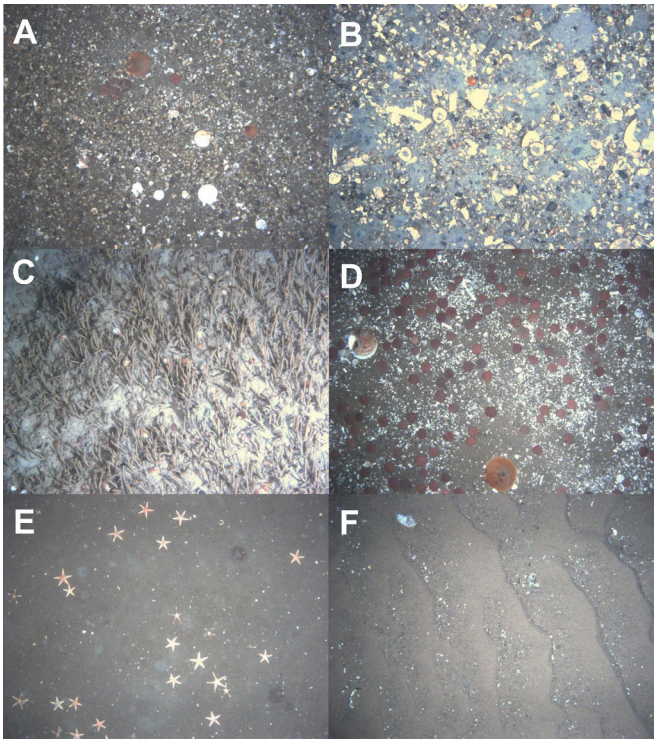

Fig. 3. Examples of habitat types included in the analysis. (A) Gravel. (B) Gravel and shell hash. (C) Dense bryozoans. (D) Sand dollar bed with shell hash. (E) Sea star bed. (F) Sand with sand waves/ripples.

2.2. Classifying scallops by age based on size and region

Sized scallops were classified into five age classes from 0 to 4+ based on the regional von Bertalanffy growth function parameters from the 2018 scallop stock assessment by the 65th Stock Assessment Review Committee (SARC65) and the more recent growth parameters developed during research funded by the Sea Scallop Research Set-Aside (RSA) program (Mann et al., 2022; NEFSC, 2018). Seed was defined as age-0 scallops, with the size cutoff set at 25 mm (Mann et al., 2022). Age cutoffs for older classes were determined using region-specific equations for Georges Bank, the Mid-Atlantic Bight, and the Nantucket Lightship Deep regions (Table 2). Scallops in the Nantucket Lightship outside the Deep region were modeled using the Georges Bank equations as only the strong Deep-region cohort, colloquially referred to as the "Peter Pan" scallops, showed unusual growth patterns that required a specialized growth equation (NEFSC, 2018).

2.3. Modeling scallop densities by age class using habitat characteristics

Generalized additive mixed models were used to investigate relationships between scallop relative abundance by age class, expressed as density (number per m^2), and habitat characteristics based on the

Table 2
Age class cutoffs for the Mid-Atlantic Bight (MAB), Georges Bank (GB), and Nantucket Lightship Deep (NLSD) regions based on the von Bertalanffy growth function parameters from Mann et al., 2022 and SARC65 (NEFSC, 2018). The region-specific cutoffs were used to classify scallops by age class during analysis.

Age class	MAB cutoffs	GB cutoffs	NLSD cutoffs
0	< 25 mm	< 25 mm	< 25 mm
1	25 - 58 mm	25 - 49 mm	25 - 38 mm
2	58 - 91 mm	49 - 81 mm	38 - 63 mm
3	91 - 110 mm	81 - 102 mm	63 - 79 mm
4	> 110 mm	> 102 mm	> 79 mm

CMECS classifications from images (Table 1). Scallop relative abundance by age class was modeled using a Tweedie distribution with the power parameters set to 1.1, 1.3, or 1.5 in the R package "mgcv" (generalized additive model function "gam" with family = Tweedie, link = logit, and thin plate splines; Wood, 2011). A Tweedie distribution was selected because scallop density data were over dispersed and contained a high proportion of zero values (Shono, 2008; Tweedie, 1984). Habitat categories for gravel, shell hash, bryozoan, sand dollar, sea star, and sand waves (Table 1) were included as categorical fixed effects. Additional fixed effects for depth and location (easting and northing) were included as non-linear smooths, with the basis dimension for the two-dimensional location smooth adjusted to k = 16 to account for broad scale spatial autocorrelations on a scale of 10–40 km (Chang et al., 2017). Categorical factors for region (Georges Bank, Mid-Atlantic Bight, or Nantucket Lightship) and survey year were included as random effects in the models to account for differences in scallop densities by region and year that were not explained by the fixed effects.

2.4. Modeling scallop swimming behavior by age class using habitat characteristics

To investigate the relationship between scallop swimming behavior and habitat type, swimming behavior (swimming vs. not swimming) was modeled using generalized additive models with a binomial distribution in the R package "mgcv" ("gam" function with family = binomial, link = logit, and thin plate splines; Wood, 2011). Due to low numbers of swimming scallops in the age-0 and age-4+ classes, age-0 and age-1 scallops were combined for this analysis, as were age-3 and age-4+ scallops. Habitat categories for gravel, shell hash, bryozoan, sand dollar, sea star, and sand waves (Table 1) were included as categorical fixed effects. Scallop shell height, scallop density, HabCam altitude, bottom temperature, depth, and location (easting and northing) were included as non-linear smooths, with the last two included to account for spatial autocorrelation. As with the density models, random effects were included to account for unknown factors that impact swimming behavior between region and survey year. Scallop size and density have been linked to swimming behavior, which changes as scallops grow larger (Brand, 2016; Caddy, 1968). Additionally, scallops may swim as an escape response to predators, a behavior that may change in areas with higher scallop densities (Barbeau et al., 1994; Bourgeois et al., 2006; Tremblay et al., 2012). HabCam altitude could also impact swimming behavior, as potential disturbance effects from vehicle pressure waves, sounds, or light could be related to distance from the seafloor (Stoner et al., 2008).

2.5. Model selection and visualization

The Tweedie power parameters used for the density models in each age class were chosen based on the lowest Bayesian Information Criterion (BIC) scores (Schwarz, 1978; Shmueli, 2010) for the full models. All additional density models for each age class used the same power parameter. Final models for both density and swimming behavior were selected based on BIC scores as the primary criterion, with secondary consideration of Akaike Information Criterion (AIC) values (Akaike, 1973) to balance selection of models that were parsimonious but still retained useful factors. Model selection involved removing predictors with high p-values (> 0.5), followed by comparison of the remaining candidate models using BIC scores. Models having BIC scores within 10 were chosen if the AIC score was lower, the deviance explained was higher, and all factors were significant (Raftery, 1995). Model fit was assessed based on the deviance explained by each final model, and model predictions were generated using the function "predict.gam" (Wood, 2011). Relationships for categorical factor and smooths for numerical terms were plotted using the R packages "ggplot2" and "visreg" as contrast plots with the Y-axis scale based on the scale of the retained factors (Breheny and Burchett, 2017; Villanueva and Chen, 2019).

3. Results

A summary of the final data used in the models is shown in Table 3.

3.1. Scallop density models by age class

The final density models for scallops older than age-0 retained all model parameters; for age-0 scallops, sea star density was not a significant predictor (Fig. 4, Table 4). Models revealed that benthic habitat components impacted scallop densities, with consistent trends across age classes for some habitat components and trends shifting as scallops aged for other habitat components (Fig. 4). Scallop densities across all age classes increased in areas with higher gravel percentages. In contrast, scallop densities across all age classes decreased in areas with sea star and sand dollar beds or sand waves (Fig. 4). The impacts of shell and bryozoan densities changed as scallops aged (Fig. 4). Age-1 through age-4+ scallop densities were highest in areas with high shell densities, while densities of age-0 scallops peaked in areas with moderate shell densities. A shift toward a mixed preference for areas with high or low shell densities was also evident for older scallops. Densities of age-0 through age-2 scallops were highest in areas with high bryozoan densities or no bryozoans, while the densities of older scallops were highest in areas with sparse bryozoan presence.

3.2. Scallop swimming models by age class

The final models explaining the swimming behavior of scallops also varied by age class (Fig. 5, Table 5). Benthic habitat components influenced swimming behavior for age-2 scallops, with these juvenile scallops more likely to swim in the presence of bryozoans. Swimming behavior in older scallops (age 2 and up) was impacted by bottom temperature, with the highest activity observed at lower temperatures for age-2 scallops and at moderate temperatures for age-3+ scallops. HabCam altitude and scallop density consistently influenced swimming behavior (Fig. 5). Scallops were more likely to swim when the HabCam vehicle was closer to the seafloor, and older scallops (age 2 and up) were more often observed swimming in areas with lower scallop densities. Scallop size was also a predictor of swimming behavior across all age classes, with likelihood of swimming peaking for scallops with shell heights between 40 mm and 60 mm (Fig. 5).

4. Discussion

The use of towed optical vehicles for generating species-specific abundance estimates, analyzing marine population and community structures, and categorizing benthic habitats has seen significant growth in recent years (Richards et al., 2019). However, a major challenge associated with large-scale optical surveys is the difficulty of effectively annotating the vast number of images or videos they produce (Vanaki et al., 2025). This limitation has been a key driver for advancing the field of automated detection, leading to considerable progress in the development and performance of image recognition models (Shin et al., 2016). In the marine research field, many existing tools for automated image and video analysis have been tailored to specific sensors, data types, or research objectives. In contrast, the VIAME platform has introduced more comprehensive and versatile algorithmic pipelines, allowing scientists to efficiently transform imagery into valuable data (Richards et al., 2019; Vanaki et al., 2025). For this project, it was critical to use the tools in VIAME to increase our sample sizes beyond the limits of manual annotations. Scallop aggregations are patchy, and images capturing swimming scallops are relatively rare, so it was essential to analyze large volumes of data to assess how habitat characteristics and the presence of the HabCam vehicle influence scallop distributions and swimming behaviors across age classes. By incorporating automated detectors, we were able to process over 1.37 million images in less than a quarter of the time required to manually annotate 40,000 images,

Table 3
Summary of the data used in the generalized additive mixed models for scallop densities and swimming behavior by age class after merging the automated scallop detections and habitat classifications from the 2019 and 2021 HabCam V3 surveys.

Categorical factors as factor category: count				
Year	2019: 576,687	2021: 793,203		
Region	GB: 448,999	MAB: 676,781	NLSD: 244,110	
GravelScore	Sand: 1,318,766	Gravelly: 35,410	Gravel: 15,714	
ShellScore	NoShell: 365,747	SparseShell: 650,376	Shell: 304,542	DenseShell: 49,225
BryozoanScore	NoBryozoans: 58,576	SparseBryozoans: 603,024	Bryozoans: 692,711	DenseBryozoans: 15,579
SandDollarScore	NoSandDollars: 1,161,979	SandDollarBed: 207,911		
SeaStarScore	NoSeaStars: 1,349,690	SeaStarBed: 20,200		
WaveScore	NoSandWaves: 1,211,380	SandWaves: 158,510		
Age 0–1 scallopClass	live_sea_scallop: 73,013	swimming_sea_scallop: 279		
Age 2 scallopClass	live_sea_scallop: 53,981	swimming_sea_scallop: 432		
Age 3–4 scallopClass	live_sea_scallop: 455,850	swimming_sea_scallop: 105		
Continuous variables as mean (minimum - maximum)				
FOV	1.004 (0.161–4.916)			
Altitude	2.048 (0.820–2.990)			
Depth	67.52 (25.790–112.270)			
Bottom temperature	9.185 (6.430–22.780)			
AgeClass0NumPerM2	0.025 (0–33.608)			
AgeClass1NumPerM2	0.033 (0–18.370)			
AgeClass2NumPerM2	0.041 (0–23.518)			
AgeClass3NumPerM2	0.097 (0–54.423)			
AgeClass4NumPerM2	0.253 (0–43.384)			
AllNumPerM2	0.449 (0–67.122)			

enabling the resolution necessary to detect environmentally driven patterns in scallop distribution and swimming behavior.

4.1. Habitat structure and settlement influences scallop densities

Scallop density trends are influenced by multiple factors, including physical aggregation during the larval stage, substrate selection at settlement, differential mortality in the post-larval stage, and juvenile movement (Thouzeau et al., 1991). Research has shown that sea scallop spat attach to benthic features such as bryozoans, hydrozoans, shell fragments, and sand grains (Brand, 2016; Thouzeau et al., 1991). Early literature on Atlantic sea scallops noted their strong habitat preference for gravel and shell hash, with juvenile scallops found in higher numbers on these bottom substrate types (Bourgeois et al., 2006; Thouzeau et al., 1991). Our model results are consistent with these observations, indicating that juvenile scallops exhibit a strong preference for gravel habitats, with that preference continuing across the age classes included in our models. Our model results also indicated a preference for habitat with moderate to dense shell hash for all age classes. This pattern may be driven by the higher survival rates of scallops on gravel or shell hash substrates (Stokesbury, 2000), which provide protection from predators, allow sufficient water flow around the individuals, and offer a relatively stable substrate for settlement, particularly in areas with strong tidal currents (Bourgeois et al., 2006, Thouzeau et al., 1991).

Because scallop spat preferentially settle in complex habitats on filamentous materials, including epifauna such as bryozoans and hydroids (Bradshaw et al., 2003; Brand et al., 1980; Harvey et al., 1997; Howarth et al., 2011; Stokesbury and Himmelman, 1995), higher densities of age-0 scallops would be expected in areas with high bryozoan cover. Recent studies on great scallops (*Pecten maximus*) and queen scallops (*Aequipecten opercularis*) in the United Kingdom demonstrated a strong preference among spat for upright, three-dimensional macroalgae. However, this association appears to weaken in adult scallops (Howarth et al., 2011), suggesting that macroalgal habitats may become less suitable or less preferred as scallops mature. This is consistent with our findings, which show a decline in scallop density with increasing bryozoan cover in age-3 and age-4 individuals (Fig. 4). As scallops grow and disperse from their initial settlement locations, additional factors such as competition for space and food resources or water flow effects on feeding efficiency may impact their distributions. Sea scallops and bryozoans are suspension feeders and may compete directly for phytoplankton and other food particles of similar sizes (Best and Thorpe, 1994; Okamura, 1990; Shumway et al., 1987). Furthermore, bryozoan aggregations may alter local hydrodynamics. Sea scallop feeding is most efficient under moderate flow conditions, with feeding rates reduced at low and high flow speeds (Pilditch and Grant, 1999; Wildish et al., 1987; Wildish and Saulnier, 1992), which in turn can limit growth (Kirby-Smith, 1972; Wildish et al., 1987). Although the impacts of dense bryozoan aggregations on scallop growth and feeding efficiency have not been directly studied, the influence of bryozoans on water flow has been documented. As with scallops, moderate flow rates are optimal for bryozoan feeding and growth (Arkema, 2009; Okamura, 1990). Dense bryozoan aggregations have been shown to reduce flow rates and increase turbulence near the seafloor (Okamura, 1984), with lower growth rates associated with reduced feeding rates in slow flow regimes (Okamura, 1988, 1992).

4.2. Hydrodynamic features and feeding behavior

Beyond biological structures, physical seabed features such as sand waves and ripples also play a role in shaping scallop distribution and survival. Although literature on sea scallops in sand wave habitats is sparse, it is known that highly dynamic habitats can disrupt larval settlement, reduce habitat stability, and limit feeding opportunities. The lower abundance of all scallops age classes in areas with sand waves and ripples is consistent with known flow-related feeding limitations. Flow speeds exceeding 10 cm/s can inhibit scallop feeding rates (Pilditch and Grant, 1999; Wildish et al., 1987; Wildish and Saulnier, 1992), while sand waves and ripples are typically formed when current speeds are over 12 cm/s (Amos et al., 1988; Passchier and Kleinhans, 2005). Even moderately elevated flow rates coupled with high turbidity have been shown to negatively impact growth, movement, and feeding in both juvenile and adult scallops (Eckman et al., 1989). Collectively, these findings indicate that environments dominated by sand waves are likely suboptimal for sea scallops at all life stages, which aligns with our finding that the presence of sand waves was associated with lower overall density in all age classes. Given the scarcity of literature regarding the ability of sea scallops to survive and thrive in sand wave habitats, automated detectors are needed to better identify and quantify scallop abundance, distribution, and behaviors in these sparsely settled

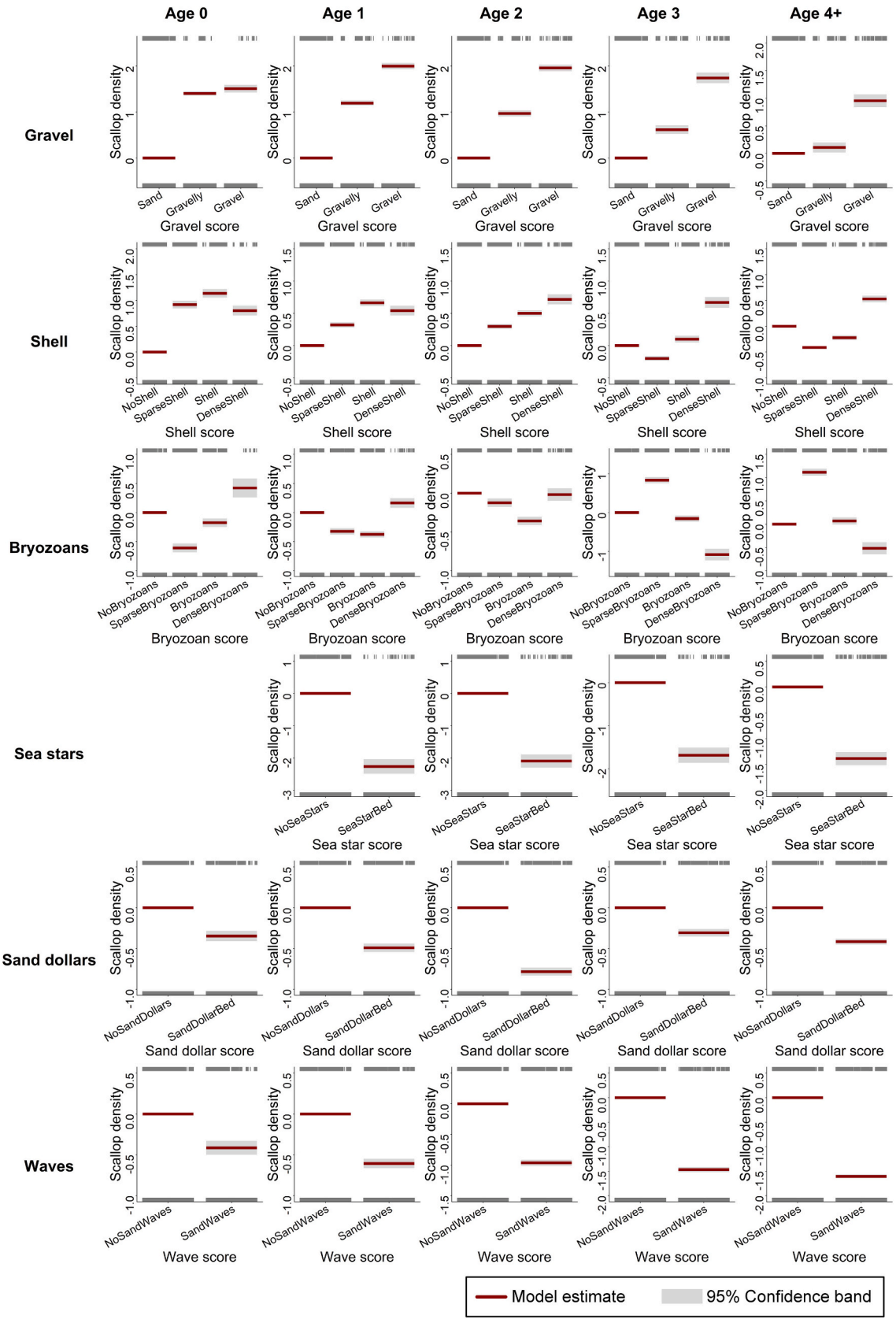

Fig. 4. Predicted smooth terms for each final scallop density model with 95 % confidence bands. The model smooths are contrast plots with the Y-axis based on the scale of the factors retained in the models (Breheny and Burchett, 2017). The rug plot on the top axis summarizes data points with positive residuals, while the rug plot on the bottom axis summarizes data points with negative residuals.

Table 4
Summary of the Tweedie generalized additive mixed models of scallop density (number/m^2) for ages 0, 1, 2, 3, and 4 and up. The Tweedie power parameters for each age class are shown with the age-class heading. The final model, model with the lowest BIC score, model with the lowest AIC score, and the full model are shown for each age group, as well as the model with only the location effect included to account for spatial autocorrelation. (BIC=Bayesian Information Criteria score, AIC = Akaike Information Criteria, Loc = location spatial correlation factor based on easting and northing, D = depth).

Scallop density (Tweedie distribution) N = 1,369,890 images					
Full model: Density ~ f(Location) + f(Depth) + Gravel + Shell + Bryozoans + Sea stars + Sand dollars + Sand waves + f(Region) + f(Year)					
Model type	Model fixed effects	Predicted scallop density range (mean) scallops/m^2	BIC	AIC	Deviance explained
Age 0 (Tweedie 1.1)					
Final and Low BIC	f(Loc) + f(D) + Gravel + Shell + Bryozoans + Sand dollars + Sand waves + f(Region) + f(Year)	0–0.802 (0.025)	265,215.6	264,815.6	17.8 %
Full and Low AIC	Full model	0–0.804 (0.025)	265,225.3	364,813.2	17.8 %
Spatial only	f(Loc)	0–0.131 (0.025)	276,205.4	275,999.6	12.1 %
Age 1 (Tweedie 1.1)					
Final, Low BIC, Low AIC, and full model	Full model	0–7.665 (0.033)	309,393.7	308,981.8	25.7 %
Spatial only	f(Loc)	0–0.253 (0.033)	337,684.2	337,478.2	14.0 %
Age 2 (Tweedie 1.1)					
Final, Low BIC, Low AIC, and full model	Full model	0–3.133 (0.041)	397,042.0	396,629.8	19.9 %
Spatial only	f(Loc)	0–0.232 (0.041)	414,544.6	414,338.6	13.8 %
Age 3 (Tweedie 1.3)					
Final, Low BIC, Low AIC, and full model	Full model	0–5.640 (0.092)	555,405.5	555,017.3	37.9 %
Spatial only	f(Loc)	0–0.987 (0.096)	590,392.2	590,186.2	27.0 %
Age 4+ (Tweedie 1.3)					
Final, Low BIC, Low AIC, and full model	Full model	0–9.689 (0.238)	878,634.6	878,222.2	53.5 %
Spatial only	f(Loc)	0–3.071 (0.244)	948,118.6	947,912.5	42.5 %

areas. Such tools can support comprehensive understanding of scallop habitat preferences, movement, and population dynamics in high-energy environments.

4.3. Predator distributions and biotic interactions

Scallop densities for ages 1 and up were lower in the presence of sea star aggregations, a result that is supported by other research on the relationship between these invertebrate groups. Some sea star species are recognized as major predators of sea scallops, with *Astropecten americanus* and *Asterias* spp. being the two most abundant sea star predators in this region. Sand stars (*A. americanus*) feed on small invertebrates including juvenile scallops (Adebola et al., 2022; Hart, 2006; Shank et al., 2012), while common (*Asterias vulgaris*) and Forbes' sea stars (*A. forbesi*) can feed on both juvenile and larger scallops because they evert their stomachs when eating (Hart, 2006; Wong and Barbeau, 2003). The distributions of sea stars can correlate with depths that overlap with scallop beds, with *Asterias* spp. found in shallow depths and *A. americanus* found in deeper waters (Shank et al., 2012). Evidence from scallop dredge surveys in the Mid-Atlantic Bight suggest that high *A. americanus* densities reduced recruitment of 40 to 88 mm scallops (i.e., overlapping age-1 and age-2 scallops in this study) (Hart, 2006; Shank et al., 2012), while effects of high *Asterias* spp. densities were unclear, with the relationships to scallop abundance shifting if the model spatial framework was changed (Shank et al., 2012). Drop camera surveys on Georges Bank concluded that abundance of all sea star species is weakly associated with abundance of scallops across all size classes (Rosellon-Druker and Stokesbury, 2019), with authors hypothesizing that active movement of *Asterias* spp. to areas with scallops (Marino II et al., 2009) impacts this relationship. Like the drop camera data, our automated detector models did not differentiate between sea star species, and the images included *Asterias* spp., *A. americanus*, and other sea star species like *Leptasterias tenera* and *Henricia sanguinolenta* with unknown relationships to sea scallops. Due to the likelihood that *A. americanus* and *Asterias* spp. may impact sea scallop populations in different ways, future efforts to develop automated detectors should prioritize species-level identification of sea star species. Improved taxonomic resolution will be critical for assessing the magnitude and variability of sea star impacts on scallop populations.

Sand dollar beds also negatively influenced scallop densities, with the effect becoming more evident for scallops age 2 and older. Similarly, other camera-based surveys have concluded that sand dollar abundance is negatively correlated with scallop abundance (Rosellon-Druker and Stokesbury, 2019). Sand dollars are not documented scallop predators, but due to their dense aggregations on scallop grounds, they may impact scallop distributions (Rosellon-Druker and Stokesbury, 2019). Potential

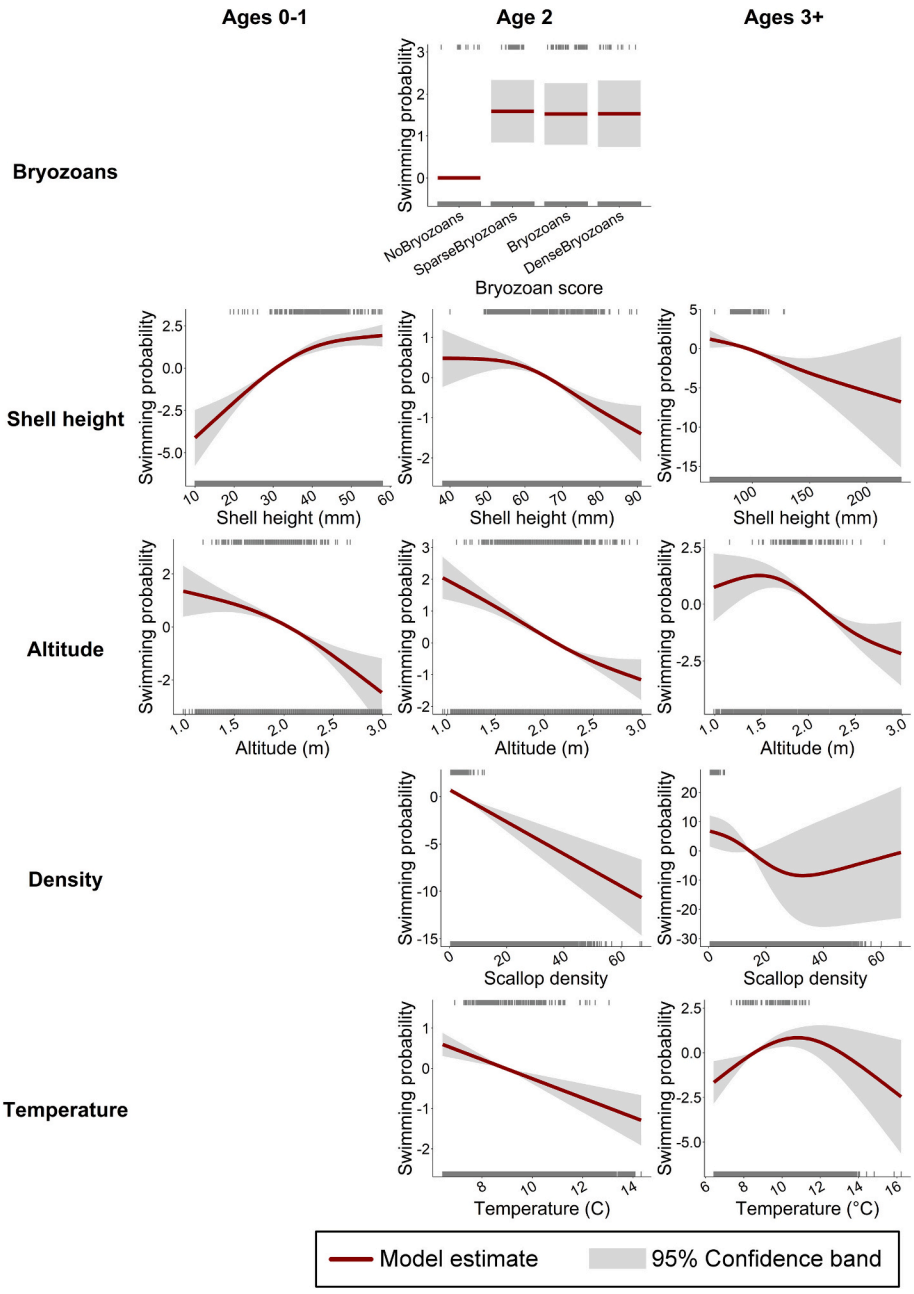

Fig. 5. Predicted smooth terms for each final model for scallop swimming probability with 95 % confidence bands. The model smooths are contrast plots with the Y-axis based on the scale of the factors retained in the models (Breheny and Burchett, 2017). The rug plot on the top axis summarizes data points with positive residuals, while the rug plot on the bottom axis summarizes data points with negative residuals.

mechanisms include competitive exclusion for space (Rosellon-Druker and Stokesbury, 2019), changes in sediment structure, and alteration of near-bottom food resources due to bioturbation and deposit-feeding activities (Cleveland and Pomory, 2022; Lawrence, 1982). Dense sand dollar beds may also act as indicators of sandy habitats that are less favorable for scallop settlement and survival compared to gravel or shell substrates (Bourgeois et al., 2006; Thouzeau et al., 1991). Therefore, the observed negative association in our models likely reflects habitat interactions rather than direct predation. Future work that incorporates finer-scale habitat descriptors coupled with sand dollar distribution data could help determine whether sand dollars actively influence scallop distributions through competition or if their presence primarily signals habitat types where scallops are less successful.

4.4. Swimming behavior

Our models predicted that scallops are more likely to swim in areas with lower scallop densities. Swimming is atypical among bivalve mollusks and is most often exhibited by juvenile scallops. The primary function of swimming in juveniles is to evade predation, while for older scallops, swimming is more likely to serve as a reproductive function, such as aggregating to enhance fertilization success (Stokesbury, 2000). Scallop shells become thicker as they grow, providing increased protection against predators, and swimming ability diminishes with increased shell heights (Brand, 2016). Studies have shown that juvenile scallops swim in response to predators, and predator densities can increase in areas with higher densities of scallops (Barbeau et al., 1994; Bourgeois et al., 2006; Tremblay et al., 2012). If juvenile scallops swim to relocate to more favorable areas, they may move from low-density

Table 5
Summary of the binomial generalized additive models for the swimming probability of scallops in age classes 0 through 1, 2, and 3 and up. The final model, model with the lowest BIC score, model with the lowest AIC score, and the full model are shown for each age group. (BIC=Bayesian Information Criteria score, AIC = Akaike Information Criteria, Loc = location spatial correlation factor based on easting and northing, D = depth, SH = shell height, Alt = HabCam altitude, Dens = scallop density, BT = bottom temperature).

Scallop swimming behavior (binomial distribution)				
Full model: Swimming probability ~ *f*(Location) + *f*(Depth) + Gravel + Shell + Bryozoans + Sea stars + Sand dollars + Sand waves + *f*(Shell height) + *f*(Altitude) + *f*(Density) + *f*(Bottom temperature) + *f*(Region) + *f*(Year)				
Model type	Model fixed effects	BIC	AIC	Deviance explained
Ages 0 and 1				
Final and Low BIC	*f*(Loc) + *f*(D) + *f*(SH) + *f*(Alt) + *f*(Region) + *f*(Year)	2971.9	2751.9	26.2 %
Low AIC	*f*(Loc) + *f*(D) + Shell + *f*(SH) + *f*(Alt) + *f*(Dens) + *f*(BT) + *f*(Region) + *f*(Year)	3008.5	2740.2	26.8 %
Full	Full model	3096.5	2746.9	27.1 %
Age 2				
Final	*f*(Loc) + *f*(D) + Bryozoans + *f*(SH) + *f*(Alt) + *f*(Dens) + *f*(BT)	4570.0	4336.1	15.0 %
Low BIC	*f*(Loc) + *f*(D) + *f*(SH) + *f*(Alt) + *f*(Dens) + *f*(BT)	4560.6	4357.2	14.4 %
Low AIC	*f*(Loc) + *f*(D) + Shell + Bryozoans + *f*(SH) + *f*(Alt) + *f*(Dens) + *f*(BT)	4594.2	4322.4	15.4 %
Full	Full model	4646.2	4322.9	15.6 %
Age 3+				
Final and Low AIC	*f*(Loc) + *f*(D) + *f*(SH) + *f*(Alt) + *f*(Dens) + *f*(BT)	1550.6	1316.4	35.3 %
Low BIC	*f*(Loc) + *f*(D) + *f*(SH) + *f*(Alt) + *f*(Dens)	1542.4	1324.4	34.7 %
Full	Full model	1679.5	1326.3	35.9 %

areas into denser aggregations to reduce predation risk. Prey species may reduce individual predation risk through the dilution effect, whereby individuals aggregate into larger or denser groups to lower their likelihood of being targeted (Frommen et al., 2009; Ydenberg and Dill, 1986). Tethering experiments have shown that the predation risk to individual scallops decreases in scallop beds relative to areas outside of these denser aggregations (Stokesbury and Himmelman, 1995), supporting this hypothesis.

4.4.1. Swimming behavior and temperature

Both biotic and abiotic factors impact the movement patterns of scallops, including temperature, depth, substrate type, currents, food availability, turbidity, salinity, and the presence of competitors and predators (Brand, 2016). In our study, bottom temperature emerges as an important predictor of swimming behavior in older juvenile and adult scallops, with swimming likelihood peaking at low temperatures for age-2 scallops and moderate temperatures for age-3+ scallops. Both age classes of scallops were less likely to swim at high temperatures, a result that agrees with research demonstrating that scallop valve muscle contractions decrease in higher temperatures (Guderley et al., 2009). The relationship between swimming behavior and temperature becomes complex at lower temperatures. Previous research has shown that the influence of temperature on valve claps, as a proxy for swimming behavior, changes depending on the history of the scallop environment (Guderley et al., 2009). For juvenile scallops collected during late May, valve claps can decrease as temperatures rise (Guderley et al., 2009), an observation that corresponds to our results for the swimming behavior of juvenile scallops that we surveyed during June and July.

Atlantic sea scallops exhibit a distinct seasonal pattern in swimming activity, but this pattern may be due to temperature in combination with other factors like food availability or energetic investments in reproduction, with spawned adult scallops swimming less frequently (Guderley and Tremblay, 2016). In Canadian waters off New Brunswick, swimming activity intensifies in spring and summer, reaching a peak in late summer and early fall, coinciding with annual temperature maxima (Guderley and Tremblay, 2016; Parsons and Dadswell, 1992) and the start of the scallop spawning season (Beninger, 1987). During the surveys included in this study, the temperatures varied across survey areas, suggesting that reproductive stages of adult scallops may have varied significantly. On Georges Bank, the main spawning event is in the fall, but a second spawning event can occur in the spring (Thompson et al., 2014). The opposite pattern is observed in the Mid-Atlantic Bight, with more scallops spawning in the spring (Kirkley and DuPaul, 1991). Temperature impacts the timing and proportion of adults that spawn during both spring and fall events (Thompson et al., 2014). Since our surveys take place between two spawning events, it is likely the adult scallop population was a mix of scallops that had recently spawned and were less likely to swim, and scallops that were preparing to spawn and more likely to swim. As a result, factors related to bottom temperature, particularly reproductive stage, may have impacted the swimming behavior of the age 3+ scallops, complicating the interpretation of the bottom temperature effect. Disentangling the relative influence of temperature from reproductive and seasonal factors may be critical for fully understanding the environmental drivers of scallop swimming behavior.

4.4.2. Habitat complexity and swimming behavior

The presence of bryozoans significantly increased swimming probability for age-2 scallops. While direct studies on scallop swimming in relation to bryozoans are lacking, this pattern is consistent with research showing that habitat complexity strongly influences scallop behavior and survival (Wong and Barbeau, 2003). Structural habitat complexity may both shelter intermediate-sized scallops and increase predation risk by supporting higher densities of predators such as sea stars or crabs (Wong et al., 2006). Predation risk in heterogeneous habitats is not uniform across scallop sizes. Smaller juvenile scallops are often able to shelter more effectively within complex substrates, while larger juveniles are more exposed and easier for predators to locate. For instance, when given a choice of prey sizes, rock crabs preferentially target larger juvenile scallops, which are easier to capture and handle within structured habitats (Wong and Barbeau, 2003). Additionally, age-2 scallops are large enough to swim effectively, but not yet so heavy-shelled that the energetic costs outweigh the benefits. Swimming at this stage can improve survival by allowing scallops to move away from predators or unsuitable microhabitats, while younger scallops rely more heavily on crypsis and byssal attachment. In bryozoan-rich patches, the trade-off may favor active movement for individuals of this age.

4.4.3. Behavioral responses to survey vehicles

These patterns in swimming behavior highlight the sensitivity of juvenile scallops to environmental conditions such as substrate type and habitat complexity. Given this behavioral plasticity, it is likely that external disturbances, particularly those that alter the local environment or introduce unfamiliar stimuli, may also influence scallop behavior. One potential source of notable disturbance could be the effect of underwater vehicles used in benthic surveys. Several studies have noted changes in behavior of marine species due to disturbance from underwater vehicles, although the level of disturbance varies greatly by species and factors such as depth, ambient light, and type of disturbance (Lorance and Trenkel, 2006; Stoner et al., 2008). More recent studies have noted the importance of vehicle altitude and speed on the strength of behavioral responses to underwater vehicles, with slower speeds and higher altitudes eliciting weaker behavioral responses (Campbell et al., 2021). The target altitude for the HabCam V3 during the years covered in this paper generally ranged from 1.52 to 2 m above the seafloor,

although usable images can be found as low as 0.5 m and as high as 3.0 m above the seafloor. We found that scallops exhibited stronger swimming responses at lower vehicle altitude, which aligns with other studies on the impacts of underwater vehicle impacts on marine species.

5. Conclusions

Optical surveys conducted for marine habitat and stock assessments collect vast amounts of data. Until recently, these datasets were typically analyzed using small subsets assumed to represent the entire dataset (L'heureux et al., 2017). Increased accessibility of machine learning techniques and decreases in the cost of powerful computers have allowed researchers to analyze much larger datasets than were previously accessible with standard tools. By using automated detectors, we were able to investigate how benthic habitat characteristics affect large numbers of individual scallops across multiple age classes, revealing changes in the impacts of these characteristics as scallops transition from newly settled juvenile to adult stages. Large-scale data analysis tools such as VIAME have allowed small organizations like ours to quickly analyze millions of images in a short time span, while the average annotations completed manually typically range from 15,000–40,000 each year. The importance of understanding factors that impact scallop recruitment, survival, and habitat preferences has increased in recent years as Atlantic sea scallop landings have declined and assessment surveys have noted substantially decreased biomass. Future efforts to analyze large existing datasets from optical surveys should be encouraged, as these databases hold a wealth of information necessary to better understand and sustainably manage valuable commercial species and ecological resources.

CRediT authorship contribution statement

Liese A. Siemann: Writing – review & editing, Writing – original draft, Visualization, Project administration, Methodology, Investigation, Funding acquisition, Formal analysis, Data curation, Conceptualization. **Matthew Dawkins:** Writing – review & editing, Software, Project administration, Methodology, Funding acquisition. **Luisa M. Garcia:** Writing – review & editing, Writing – original draft, Investigation, Funding acquisition. **Jonathan Crall:** Writing – review & editing, Software. **Tasha E. O'Hara:** Writing – review & editing, Writing – original draft, Project administration, Investigation, Funding acquisition, Data curation.

Declaration of competing interest

The authors declare that they have no known competing financial interests or personal relationships that could have appeared to influence the work reported in this paper.

Acknowledgments

We would like to thank our many colleagues at CFF and Kitware for their participation in HabCam surveys and VIAME model development. We are grateful to the vessel owners, operators, and crew members who made this project possible. We thank our anonymous reviewers for comments that improved the manuscript. This research was funded by the NOAA Sea Scallop Research Set-Aside grants NA19NMF4540016, NA19NMF4540017, NA19NMF4540018, NA21NMF4540016, and NA21NMF4540018. The funders had no role in study design. Coonamessett Farm Foundation, Inc., is a nonprofit scientific research foundation.

Appendix A. The Habitat Mapping Camera (HabCam) V3 towed camera system

A.1. Background of the HabCam vehicles

The HabCam V3, developed by the Woods Hole Oceanographic Institution, represents the third generation in a series of advanced, non-lethal underwater survey systems (Howland et al., 2006). Designed in collaboration with the commercial scallop industry, HabCam V3 enables ecosystem-based surveys targeting Atlantic sea scallops and their associated benthic habitats.

This optical imaging system was developed as an alternative to traditional dredge-based sampling methods, which are often limited by issues such as gear escapement, overfilling, and habitat disturbance. The adoption of non-invasive optical tools like HabCam has significantly improved the accuracy and efficiency of benthic ecosystem monitoring by providing high-resolution imagery without physically disrupting the seafloor.

A.2. HabCam V3 system overview

HabCam V3 is a towed, dual-camera imaging system designed for high-resolution benthic habitat surveys (Fig. 6). The vehicle frame is built with hollow steel and measures 3.175-m in length × 1.651-m in width × 1.168-m in height. The cameras are mounted to capture overlapping stereo images with depth disparities appropriate for measuring organisms the size of sea scallops (Fig. 6B). These stereo images can be processed into three-dimensional renderings, which are viewable using appropriate software or 3D glasses (Fig. A2). The vehicle is deployed from commercial vessels and towed via a triple-armored fiber-optic cable operated with a hydraulic winch. This cable encloses single-mode optical fibers and electrical conductors, enabling real-time data transmission and precise vehicle control.

A.2.1. System components

Because the HabCam V3 is a modular system, components can be upgraded as needed. The previous and current imaging system components and sensors are described in Table A1.

Table A1. HabCam V3 components.

System	Component (details)	2017–2023 Specifications/models	2024–2025 Specifications/models
Imaging system	Cameras	Two GE Prosilica 1.3 MP digital cameras	Two Manta G-319C 3.2 MP digital cameras
	Lighting	Four VIGI-Lux MVS-5002 xenon strobe lamps	Four Artic Rays Dragonfish mini-LED strobes
	Synchronization (of image capture and strobing)	Gardasoft CC320 IP timing controller	Removed – trigger built into camera software
Environmental sensors	Conductivity, temperature, and depth (CTD) sensor	Sea-Bird Electronics SBE 37-SI CTD sensor	Sea-Bird Electronics SBE 37-SI CTD sensor

(*continued on next page*)

(*continued*)

System	Component (details)	2017–2023 Specifications/models	2024–2025 Specifications/models
	Attitude (heading, pitch, and roll) sensor	Microstrain 3DM-GX3–25 inertial measurement unit	Microstrain 3DM-GX3–25 inertial measurement unit
	Altimeter (height above the sea floor)	Teledyne Benthos PSA-916 sonar altimeter	Teledyne Benthos PSA-916 sonar altimeter
	Front-facing sonar		Teledyne Benthos BlueView M450

A.2.2. Data integration

Sensor data, along with vessel location coordinates and depth information, are integrated and managed onboard the HabCam server. External sensors are connected via SubConn underwater connectors, ensuring modularity and reliable operation in a marine environment. Each image is automatically embedded with time-synchronized metadata, including vehicle and vessel sensor outputs (e.g., position, depth, heading).

A.3. At-sea operations

The HabCam V3 system is towed along continuous, pre-defined tran*sec*ts that follow bathymetric contours across the seafloor. The spacing between transects is variable and determined by management objectives, habitat complexity, and the expected abundance and spatial distribution of target species. The operational parameters for conducting HabCam V3 surveys are shown in Table A2.

Table A2. HabCam V3 operational parameters.

Operational parameters	Typical values	Notes
Altitude	1.5–2.6 m	Results in fields of view from 1.6 to 3.5 m^2 (current cameras)
Towing speed	4.5–5.5 knots	
Image acquisition rate	4–6 stereo image pairs per sec	
Data transmission	Continuous	Real-time transmission over the armored fiber-optic cable
Transect spacing	2–5 nm	

A custom onboard graphical user interface (GUI) displays down-sampled images alongside real-time environmental and vehicle data, including salinity, benthic temperature, and altitude. This interface enables pilots to actively monitor and control the vehicle during survey operations. HabCam altitude is controlled via a joystick-operated winch system, which adjusts the length of the optical cable connecting the vehicle to the towing vessel.

A.4. Image annotation and data processing

Recently, the HabCam V3 system has undergone a multi-year upgrade (see Table A1), resulting in a lower image acquisition rate and improved image resolution. During typical 24-h survey operations, the HabCam V3 system collects four images per second, resulting in approximately 300,000 paired stereo images, generating approximately 3 TB of image data per day. Prior to 2023, the V3 collected 5–6 images per second of lower resolution imagery, which generated over 500,000 paired images, and 3 TB of data per day. To facilitate standardized spatial coverage, each "station" (i.e., a single image) is selected at a fixed interval along the track. In past years, annotation rates have varied depending on project and available resources, with stations ranging between 40 and 180 m apart.

Image annotation is conducted manually by trained analysts using a customized, open-source annotation platform developed by the Visual Geometry Group (VGG) at the University of Oxford (Dutta and Zisserman, 2019). For each image, analysts record key biological and environmental features, including sea scallop counts and measurements, presence of ecologically or commercially significant species and behaviors, and dominant or mixed sediment types.

These data inputs are combined and included as metadata attached to each image to simplify comprehensive analysis of data in the images and sensor parameters.

Image annotations are integrated with corresponding image metadata for analysis. Image field of view (FOV) is calculated based on the camera specifications and the vehicle altitude, pitch, and roll. Salinity is derived from in situ conductivity and temperature measurements collected by the Seabird CTD sensor, using internationally recognized equations for the calculation of practical salinity (Pritchard, 1982). Densities of annotated organisms, including scallops, are calculated based on organism counts within the image divided by the image FOV.

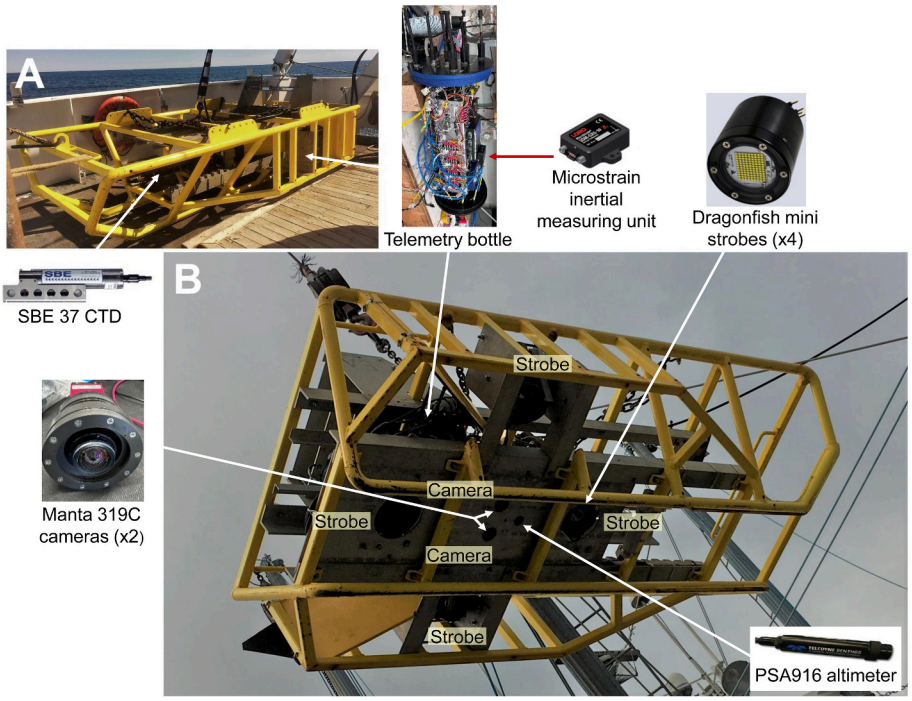

Fig. A1. HabCam V3 with labeled system components. (A) Side view. (B) Bottom view.

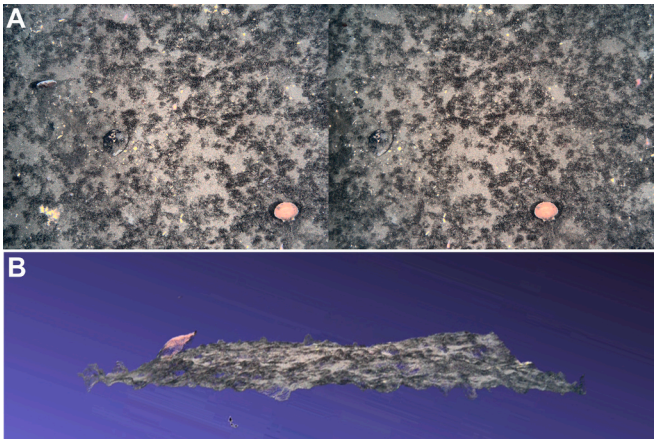

Fig. A2. (A) Example of a stereo pair of images. (B) 3D model from the image pair viewed in MeshLab (Cignioni et al., 2011) showing a swimming scallop and the sediment cloud it generated when jetting off the sea floor. Note that the scallop in the upper left corner is not included in the 3D rendering because it is present in only one of the images.

Appendix B. Scallop detectors and habitat classifiers in Video and Image Analytics for Marine Environments (VIAME)

B.1. Scallop detectors

Scallop detectors are available in the VIAME toolkit as part of the web application and Windows and Linux installation packages. These detectors were trained using scallop annotations from HabCam V3 surveys conducted in 2017 through 2020 and HabCam V4 surveys conducted in 2015 and 2016 by the National Marine Fisheries Service Northeast Fisheries Science Center (NEFSC).

The scallop model was built from an ensemble of three separately trained detectors using the Cascade R-CNN (Cai and Vasconcelos, 2018), YOLOv7 (Wang et al., 2023), and HR-Net (Wang et al., 2020) neural net architectures. The Cascade R-CNN and YOLOv7 models were trained in a one-class configuration for all scallop categories, and the HR-Net models were trained for four scallop classes including live, swimming, and dead scallops plus clappers (i.e., empty scallop shells with intact hinges). To enhance classification, a secondary four-class classifier trained with the EfficientNetV2 neural network (Tan and Le, 2021) was applied on top of the combined Cascade R-CNN and HR-Net detections to produce an additional layer of refined predictions. The four models were fused into a single output via a weighted box fusion technique (Solovyev et al., 2021), taking a combination of each detector when they had sufficient intersection-over-union overlap, with higher weights applied to the reclassified EfficientNetV2 detections because these detectors had the highest mean average precision scores. The final fused multi-class scallop detectors have mean average precision scores of 0.71 to 0.93 during test evaluations, which are all within the range of excellent scores for general use object detectors.

Scallop measurements were incorporated into the detector models using tight bounding boxes around scallops. The length of the longest side was treated as the scallop length because scallop shell widths are less than shell heights for most sizes. That length in pixels was converted to mm based on

the camera field of view derived from the three-dimensional position of the camera off the sea floor (e.g., based on the HabCam vehicle altitude off bottom, pitch, and roll) and the camera intrinsic properties (e.g., the camera pixel size, sensor size in pixels, and focal length). Because the shell widths of scallops over 160 mm tend to be larger than their shell heights, the measurements based on the longest side of the bounding box are likely to be shell widths. Therefore, the estimates for these large scallops were converted from widths to heights using the standard equation for this conversion from scallop stock assessments (NEFSC, 2018).

B.1.1. Validating automated scallop measurements

To determine if the scallops detected and measured using machine learning (automated annotations) differed significantly from those identified and measured by human annotators (manual annotations), the manual and automated annotations from the images included in the 2021 scallop surveys were compared using chi-square goodness of fit tests. Scallop lengths were grouped into 5-mm length bins through the 99th percentile of the observed values in the manual annotation dataset. Similarly, scallop densities (number per square meter) were grouped into 0.25 per square meter bins through the 95th percentile, and into 1 per square meter bins through the 99th percentile of the observed densities in the manual annotation dataset.

Based on chi-square goodness of fit tests, scallop lengths and densities did not differ significantly between manual annotations and automated detections for the 2021 sea scallop data. The distributions of binned scallop lengths did not differ significantly between manual measurements and those estimated using automated detection (χ^2 (625, $N = 10{,}005$) = 648.00, $p = 0.254$). Similarly, the distributions of binned scallop densities were not significantly different between those derived from manual annotations and automated detectors (χ^2 (418, $N = 40{,}122$) = 440.00, $p = 0.220$).

B.2. Habitat classifiers

The habitat classifiers are available in the VIAME toolkit as part of the web application and Windows and Linux installation packages. These classifiers were developed from image sets collected during the HabCam V3 surveys conducted in 2018 through 2021, with categories defined based on densities or counts of habitat components (Table B1). Full image labels were applied if the substrate was consistent across the image, while subregions were outlined and labeled when the substrate within an image was patchy. Both types of annotations were combined in the training sets.

Multi-stage processes, focal loss functions, and weighted models were tested as training sets were unbalanced, with large disparities in the numbers of classified examples of different habitats. Focal loss (Lin et al., 2017) and weighted models were tested to build faster one-stage models with improved performance in a single-model solution; however, multiple models still outperformed single models developed with these additions. The final models trained with the EfficientNetV2 neural network (Tan and Le, 2021) were developed using a two-stage process, with classifiers trained across the full training dataset followed by secondary training focused on frames with uncertain initial classifications.

Habitat component models were evaluated using F1 scores, a common metric used to measure the performance of machine-learning models with imbalanced datasets (Naidu et al., 2023). Six habitat components with categories that had F1 scores over 0.50 for all categories were included in the datasets (Table B1). Multiple categories based on density were included in each model for gravel, shell hash, and bryozoans. The models for sea star beds, sand dollar beds, and sand waves were binary classifiers.

Table B1. Substrate components used for habitat classifications. The null class, the component F1-score, and the numerical values assigned within each substrate group are also shown.

Habitat component	Null category	Other categories	F1-score
Gravel	mud/sand (<5 % gravel)	gravelly (5–30 % gravel)	0.53
		gravel (>30 % gravel)	0.72
Shell	no shell hash (<5 % shell hash)	shell hash sparse (5–30 % shell hash)	0.72
		shell hash (30–80 % shell hash)	0.70
		shell hash dense (>80 % shell hash)	0.58
Bryozoans	no bryozoans (<5 % bryozoans)	bryozoans sparse (5–30 % bryozoans)	0.76
		bryozoans (30–80 % bryozoans)	0.76
		bryozoans dense (>80 % bryozoans)	0.50
Sea stars	few to no sea stars	sea star bed (>10 or > 50 % image coverage)	0.73
Sand dollars	few to no sand dollars	sand dollar bed (>10 or > 50 % image coverage)	0.83
Sand waves	no sand waves	sand waves	0.72

Data availability

Data tables and R scripts are publicly available at https://figshare.com/articles/dataset/Siemann_et_al_VIAME_scallops/30128908. The full dataset of imagery used in this study is too large to share in its entirety (> 2 TB). However, a representative set of imagery, used during model development, can be downloaded at https://viame.kitware.com/#/folder/5e4c2584a0fc86aa03120c49. VIAME installations can be downloaded from https://github.com/VIAME/VIAME#installations. The web version of VIAME is located at https://viame.kitware.com/.

References

Adebola, T., Hart, D., Chigbu, P., 2022. Bathymetric trends in the body size, and diet of *Astropecten americanus* in the Northwest Atlantic Ocean. Estuar. Coast. Shelf Sci. 269, 107814.

Akaike, H., 1973. Information theory as an extension of the maximum likelihood principle. In: Petrov, B.N., Csaki, F. (Eds.), Second International Symposium on Information Theory. Akademiai Kiado, Budapest, pp. 267–281.

Allee, R., Cicchetti, G., Finkbeiner, M., Goodin, K., Handley, L., Madden, C., 2012. Coastal and Marine Ecological Classification Standard, Version 4.0.

Amos, C.L., Bowen, A.J., Huntley, D.A., Lewis, C.F.M., 1988. Ripple generation under the combined influences of waves and currents on the Canadian continental shelf. Cont. Shelf Res. 8 (10), 1129–1153.

Arkema, K.K., 2009. Flow-mediated feeding in the field: consequences for the performance and abundance of a sessile marine invertebrate. Mar. Ecol. Prog. Ser. 388, 207–220.

Barbeau, M.A., Scheibling, R.E., Hatcher, B.G., Taylor, L.H., Hennigar, A.W., 1994. Survival analysis of tethered juvenile sea scallops *Placopecten magellanicus* in field experiments: effects of predators, scallop size and density, site and season. Mar. Ecol. Prog. Ser. 243–256.

Beninger, P.G., 1987. A qualitative and quantitative study of the reproductive cycle of the giant scallop, *Placopecten magellanicus*, in the bay of Fundy (New Brunswick, Canada). Can. J. Zool. 65 (3), 495–498.

Best, M.A., Thorpe, J.P., 1994. Particle Size, Clearance Rate and Feeding Efficiency in Marine Bryozoa. Biology and Palaeobiology of Bryozoans. Olsen and Olsen, Fredensborg, pp. 9–14.
Bourgeois, M., Brêthes, J.C., Nadeau, M., 2006. Substrate effects on survival, growth and dispersal of juvenile sea scallop, *Placopecten magellanicus* (Gmelin 1791). J. Shellfish Res. 25 (1), 43–49.
Bradshaw, C., Collins, P., Brand, A.R., 2003. To what extent does upright sessile epifauna affect benthic biodiversity and community composition? Mar. Biol. 143, 783–791.
Brand, A.R., 2016. Scallop ecology: Distributions and behaviour. In: Developments in Aquaculture and Fisheries Science, vol. 40. Elsevier, pp. 469–533.
Brand, A.R., Paul, J.D., Hoogesteger, J.N., 1980. Spat settlement of the scallops *Chlamys opercularis* (L.) and *Pecten maximus* (L.) on artificial collectors. J. Mar. Biol. Assoc. U. K. 60 (2), 379–390.
Breheny, P., Burchett, W., 2017. Visualization of Regression Models Using Visreg.
Caddy, J.F., 1968. Underwater observations on scallop (*Placopecten magellanicus*) behaviour and drag efficiency. J. Fisher. Board Canada 25 (10), 2123–2141.
Cai, Z., Vasconcelos, N., 2018. Cascade r-cnn: delving into high quality object detection. In: Proceedings of the IEEE Conference on Computer Vision and Pattern Recognition, pp. 6154–6162.
Campbell, M.D., Huddleston, A., Somerton, D., Clarke, M.E., Wakefield, W., Murawski, S., Taylor, C., Singh, H., Girdhar, Y., Yoklavich, M., 2021. Assessment of Attraction and Avoidance Behaviors of Fish in Response to the Proximity of Transiting Underwater Vehicles.
Carey, J.D., Stokesbury, K.D., 2011. An assessment of juvenile and adult sea scallop, *Placopecten magellanicus*, distribution in the Northwest Atlantic using high-resolution still imagery. J. Shellfish Res. 30 (3), 569–582.
Chang, J.H., Shank, B.V., Hart, D.R., 2017. A comparison of methods to estimate abundance and biomass from belt transect surveys. Limnol. Oceanogr. Methods 15 (5), 480–494.
Cleveland, A.B., Pomory, C.M., 2022. Movement and behavior of the sand dollar Mellita tenuis (Echinodermata: Echinoidea). Mar. Freshw. Behav. Physiol. 55 (1–2), 1–20.
Cragg, S.M., 2006. Development, physiology, behaviour and ecology of scallop larvae. In: Developments in Aquaculture and Fisheries Science, vol. 35. Elsevier, pp. 45–122.
Dawkins, M., Sherrill, L., Fieldhouse, K., Hoogs, A., Richards, B., Zhang, D., Prasad, L., Williams, K., Lauffenburger, N., Wang, G., 2017, March. An open-source platform for underwater image and video analytics. In: 2017 IEEE Winter Conference on Applications of Computer Vision (WACV). IEEE, pp. 898–906.
Dutta, A., Zisserman, A., 2019, October. The VIA annotation software for images, audio and video. In: Proceedings of the 27th ACM International Conference on Multimedia, pp. 2276–2279.
Eckman, J.E., Peterson, C.H., Cahalan, J.A., 1989. Effects of flow speed, turbulence, and orientation on growth of juvenile bay scallops Argopecten Irradians concentricus (say). J. Exp. Mar. Biol. Ecol. 132 (2), 123–140.
Frommen, J.G., Hiermes, M., Bakker, T.C., 2009. Disentangling the effects of group size and density on shoaling decisions of three-spined sticklebacks (*Gasterosteus aculeatus*). Behav. Ecol. Sociobiol. 63, 1141–1148.
Guderley, H., Labbé-Giguere, S., Janssoone, X., Bourgeois, M., Pérez, H.M., Tremblay, I., 2009. Thermal sensitivity of escape response performance by the scallop Placopecten magellanicus: impact of environmental history. J. Exp. Mar. Biol. Ecol. 377 (2), 113–119.
Guderley, H.E., Tremblay, I., 2016. Swimming in scallops. In: Developments in Aquaculture and Fisheries Science, vol. 40. Elsevier, pp. 535–566.
Hart, D.R., 2006. Effects of sea stars and crabs on sea scallop *Placopecten magellanicus* recruitment in the mid-Atlantic bight (USA). Mar. Ecol. Prog. Ser. 306, 209–221.
Harvey, M., Bourget, E., Gagné, N., 1997. Spat settlement of the giant scallop, *Placopecten magellanicus* (Gmelin, 1791), and other bivalve species on artificial filamentous collectors coated with chitinous material. Aquaculture 148 (4), 277–298.
Hennen, D.R., Hart, D.R., 2012. Shell height-to-weight relationships for Atlantic Sea scallops (*Placopecten magellanicus*) in offshore US waters. J. Shellfish Res. 31 (4), 1133–1144.
Howarth, L.M., Wood, H.L., Turner, A.P., Beukers-Stewart, B.D., 2011. Complex habitat boosts scallop recruitment in a fully protected marine reserve. Mar. Biol. 158 (8), 1767–1780. https://doi.org/10.1007/s00227-011-1690-y.
Howland, J., Gallager, S., Singh, H., Girard, A., Abrams, L., Griner, C., Taylor, R., Vine, N., 2006, September. Development of a towed survey system for deployment by the fishing industry. In: OCEANS 2006. IEEE, pp. 1–5.
Kirby-Smith, W.W., 1972. Growth of the bay scallop: the influence of experimental water currents. J. Exp. Mar. Biol. Ecol. 8 (1), 7–18.
Kirkley, J.E., DuPaul, W.D., 1991. Temporal variations in spawning behavior of sea scallops, *Placopecten magellanicus* (Gmelin, 1791), in the mid-Atlantic resource area. J. Shellfish Res. 10 (2), 389.
Lawrence, J.M., 1982. Echinoderms. CRC Press.
L'heureux, A., Grolinger, K., Elyamany, H.F., Capretz, M.A., 2017. Machine learning with big data: challenges and approaches. IEEE Access 5, 7776–7797.
Lin, T.Y., Goyal, P., Girshick, R., He, K., Dollár, P., 2017. Focal loss for dense object detection. In: Proceedings of the IEEE International Conference on Computer Vision, pp. 2980–2988.
Lorance, P., Trenkel, V.M., 2006. Variability in natural behaviour, and observed reactions to an ROV, by mid-slope fish species. J. Exp. Mar. Biol. Ecol. 332 (1), 106–119.
Mann, R.L., Rudders, D., Roman, S., Southworth, M., Clark, K.R., 2022. Age Based Assessment in the Sea Scallop *Placopecten magellanicus*: A Pilot Study-Final Report.
Marino II, M.C., Juanes, F., Stokesbury, K.D., 2009. Spatio-temporal variations of sea star *Asterias* spp. distributions between sea scallop *Placopecten magellanicus* beds on Georges Bank. Mar. Ecol. Prog. Ser. 382, 59–68.
Naidu, G., Zuva, T., Sibanda, E.M., 2023. A review of evaluation metrics in machine learning algorithms. In: Computer Science on-Line Conference. Springer International Publishing, Cham, pp. 15–25.
National Marine Fisheries Service (NMFS), 2024. Fisheries of the United States, 2022. U. S. Department of Commerce.
Northeast Fisheries Science Center (NEFSC), 2018. 65th Northeast Regional Stock Assessment Workshop (65th SAW). Assessment Report.
Okamura, B., 1984. The effects of ambient flow velocity, colony size, and upstream colonies on the feeding success of Bryozoa. I. Bugula stolonifera Ryland, an arborescent species. J. Exp. Mar. Biol. Ecol. 83 (2), 179–193.
Okamura, B., 1988. The influence of neighbors on the feeding of an epifaunal bryozoan. J. Exp. Mar. Biol. Ecol. 120 (2), 105–123.
Okamura, B., 1990. Particle size, flow velocity, and suspension-feeding by the erect bryozoans Bugula neritina and B. Stolonifera. Mar. Biol. 105 (1), 33–38.
Okamura, B., 1992. Microhabitat variation and patterns of colony growth and feeding in a marine bryozoan. Ecology 73 (4), 1502–1513.
Parsons, G.J., Dadswell, M.J., 1992. Seasonal and size-related swimming behaviour in the giant scallop, *Placopecten magellanicus*. In: Conf. Proc. Aquaculture'92: Growing Toward the 21st Century, Vol. 1992, p. 174.
Passchier, S., Kleinhans, M.G., 2005. Observations of sand waves, megaripples, and hummocks in the Dutch coastal area and their relation to currents and combined flow conditions. J. Geophys. Res.: Earth Surf. 110 (F4).
Pilditch, C.A., Grant, J., 1999. Effect of variations in flow velocity and phytoplankton concentration on sea scallop (*Placopecten magellanicus*) grazing rates. J. Exp. Mar. Biol. Ecol. 240 (1), 111–136.
Pritchard, D.W., 1982. A Summary Concerning the Newly Adopted Practical Salinity Scale, 1978, and the International Equation of State of Seawater, 1980.
Raftery, A.E., 1995. Bayesian model selection in social research. Sociol. Methodol. 111–163.
Richards, B.L., Beijbom, O., Campbell, M.D., Clarke, M.E., Cutter, G., Dawkins, M., Edington, D., Hart, D.R., Hill, M.C., Hoogs, A., Kriegman, D., 2019. Automated Analysis of Underwater Imagery: Accomplishments, Products, and Vision.
Rosellon-Druker, J., Stokesbury, K.D., 2019. Quantification of echinoderms (Echinodermata) on Georges Bank, and the potential influence of marine protected areas on these populations. Invertebr. Biol. 138 (2), e12243.
Schwarz, G., 1978. Estimating the dimension of a model. Ann. Stat. 461–464.
Shank, B.V., Hart, D.R., Friedland, K.D., 2012. Post-settlement predation by sea stars and crabs on the sea scallop in the mid-Atlantic bight. Mar. Ecol. Prog. Ser. 468, 161–177.
Shin, H.C., Roth, H.R., Gao, M., Lu, L., Xu, Z., Nogues, I., Yao, J., Mollura, D., Summers, R.M., 2016. Deep convolutional neural networks for computer-aided detection: CNN architectures, dataset characteristics and transfer learning. IEEE Trans. Med. Imaging 35 (5), 1285–1298.
Shmueli, G., 2010. To explain or to predict? Stat. Sci. 25, 289–310.
Shono, H., 2008. Application of the Tweedie distribution to zero-catch data in CPUE analysis. Fish. Res. 93 (1–2), 154–162.
Shumway, S.E., Selvin, R., Schick, D.F., 1987. Food resources related to habitat in the scallop *Placopecten magellanicus* (Gmelin, 1791): a qualitative study. J. Shellfish Res. 6 (2), 89–95.
Solovyev, R., Wang, W., Gabruseva, T., 2021. Weighted boxes fusion: Ensembling boxes from different object detection models. Image Vis. Comput. 107, 104117.
Stokesbury, K.D., 2000. Physical and Biological Variables Influencing the Spatial Distribution of the Giant Scallop *Placopecten magellanicus*, 14. Alaska Department of Fish and Game, Special Publication, EUA, pp. 13–19.
Stokesbury, K.D., Himmelman, J.H., 1995. Biological and physical variables associated with aggregations of the giant scallop *Placopecten magellanicus*. Can. J. Fish. Aquat. Sci. 52 (4), 743–753.
Stoner, A.W., Ryer, C.H., Parker, S.J., Auster, P.J., Wakefield, W.W., 2008. Evaluating the role of fish behavior in surveys conducted with underwater vehicles. Can. J. Fish. Aquat. Sci. 65 (6), 1230–1243.
Tan, M., Le, Q., 2021, July. Efficientnetv2: Smaller models and faster training. In: International Conference on Machine Learning. PMLR, pp. 10096–10106.
Thompson, K.J., Inglis, S.D., Stokesbury, K.D., 2014. Identifying spawning events of the sea scallop *Placopecten magellanicus* on Georges Bank. J. Shellfish Res. 33 (1), 77–87.
Thouzeau, G., Robert, G., Smith, S.J., 1991. Spatial variability in distribution and growth of juvenile and adult sea scallops *Placopecten magellanicus* (Gmelin) on eastern Georges Bank (Northwest Atlantic). Mar. Ecol. Prog. Ser. 205–218.
Tremblay, I., Guderley, H.E., Himmelman, J.H., 2012. Swimming away or clamming up: the use of phasic and tonic adductor muscles during escape responses varies with shell morphology in scallops. J. Exp. Biol. 215 (23), 4131–4143.
Tweedie, M.C.K., 1984. An index which distinguishes between some important exponential families. In: Statistics: Applications and New Directions. Proceedings of the Indian Statistical Institute Golden Jubilee International Conference. Indian Statistical Institute, Calcutta, pp. 579–604.
Vanaki, S., Hart, D.R., Chang, J.H., 2025. How many dollars are in the sea? Estimating sand dollar (*Echinarachnius parma*) abundance using an iteratively trained convolutional neural network and generalized additive models. Eco. Inform. 90, 103311.
Villanueva, R.A.M., Chen, Z.J., 2019. ggplot2: Elegant Graphics for Data Analysis.
Wang, C.Y., Bochkovskiy, A., Liao, H.Y.M., 2023. YOLOv7: trainable bag-of-freebies sets new state-of-the-art for real-time object detectors. In: Proceedings of the IEEE/CVF Conference on Computer Vision and Pattern Recognition, pp. 7464–7475.
Wang, J., Sun, K., Cheng, T., Jiang, B., Deng, C., Zhao, Y., Liu, D., Mu, Y., Tan, M., Wang, X., Liu, W., 2020. Deep high-resolution representation learning for visual recognition. IEEE Trans. Pattern Anal. Mach. Intell. 43 (10), 3349–3364.

Wildish, D.J., Saulnier, A.M., 1992. The effect of velocity and flow direction on the growth of juvenile and adult giant scallops. J. Exp. Mar. Biol. Ecol. 155 (1), 133–143.
Wildish, D.J., Kristmanson, D.D., Hoar, R.L., DeCoste, A.M., McCormick, S.D., White, A. W., 1987. Giant scallop feeding and growth responses to flow. J. Exp. Mar. Biol. Ecol. 113 (3), 207–220.
Wong, M.C., Barbeau, M.A., 2003. Effects of substrate on interactions between juvenile sea scallops (*Placopecten magellanicus Gmelin*) and predatory sea stars (*Asterias vulgaris Verrill*) and rock crabs (*Cancer irroratus say*). J. Exp. Mar. Biol. Ecol. 287 (2), 155–178.
Wong, M.C., Wright, L.D., Barbeau, M.A., 2006. Sediment selection by juvenile sea scallops (*Placopecten magellanicus* (Gmelin)), sea stars (*Asterias vulgaris* Verrill) and rock crabs (*Cancer irroratus* say). J. Shellfish Res. 25 (3), 813–821.
Wood, S.N., 2011. Fast stable restricted maximum likelihood and marginal likelihood estimation of semiparametric generalized linear models. J. R. Stat. Soc. Ser. B Stat Methodol. 73 (1), 3–36.
Ydenberg, R.C., Dill, L.M., 1986. The economics of fleeing from predators. In: Advances in the Study of Behavior, vol. 16. Academic Press, pp. 229–249.